Reprogrammed mRNA translation drives resistance to therapeutic targeting of ribosome biogenesis

APPENDIX

APPENDIX FIGURES

Appendix Figure S1

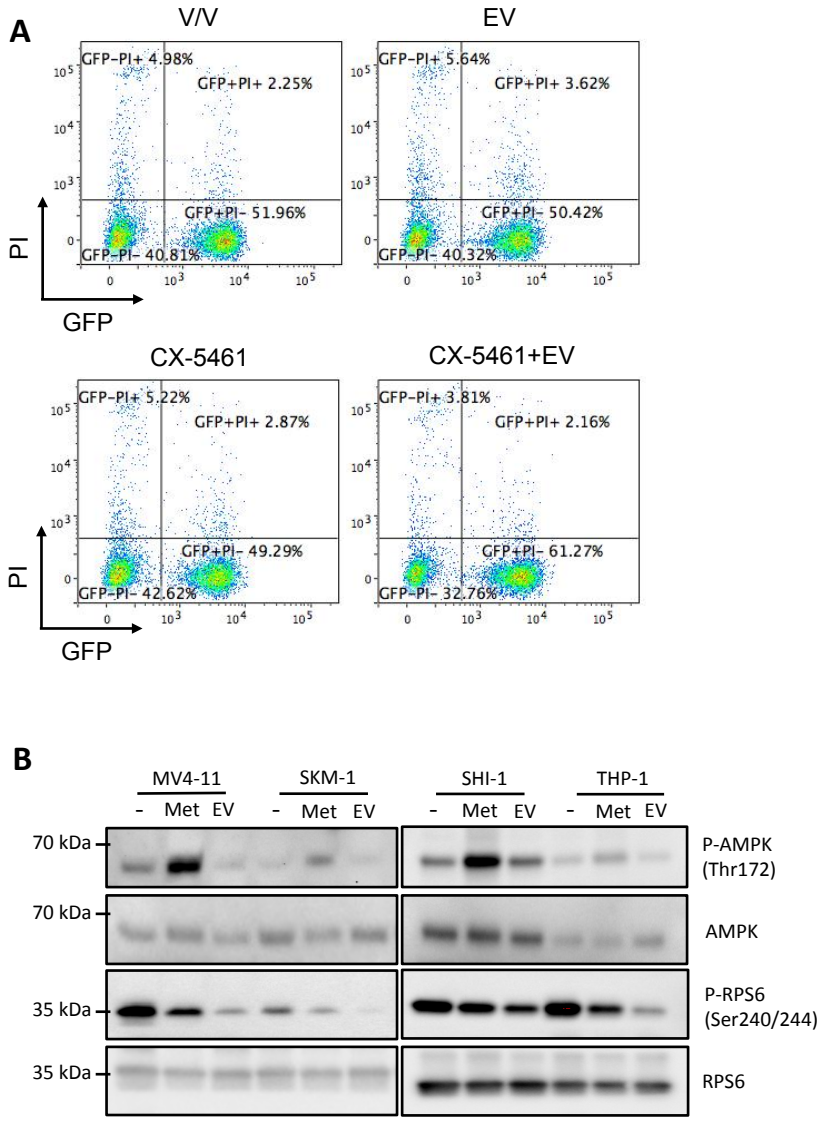

Appendix Figure S1. Investigating the mechanism(s) of acute ribosome-directed therapy

(A) C57BL/6 mice with transplanted Eμ-*Myc* (MSCV Gfp; clone #4242) B-cell lymphoma cells were treated as indicated for 2 hours. Representative flow cytometry dot-plots of the inguinal lymph nodes cells isolated from C57BL/6 mice and stained with Propidium iodide (PI). Dot-plots are representative of individual mice (n=6) per group. **(B)** Western blot analysis of phosphorylated AMPK and phosphorylated RPS6 in the indicated human acute myeloid leukemia (AML) cell lines for the on-target effect of 10 mM metformin treatment for 24 hours and 5 nM everolimus treatment for 3 hours respectively (n=2).

Appendix Figure S2

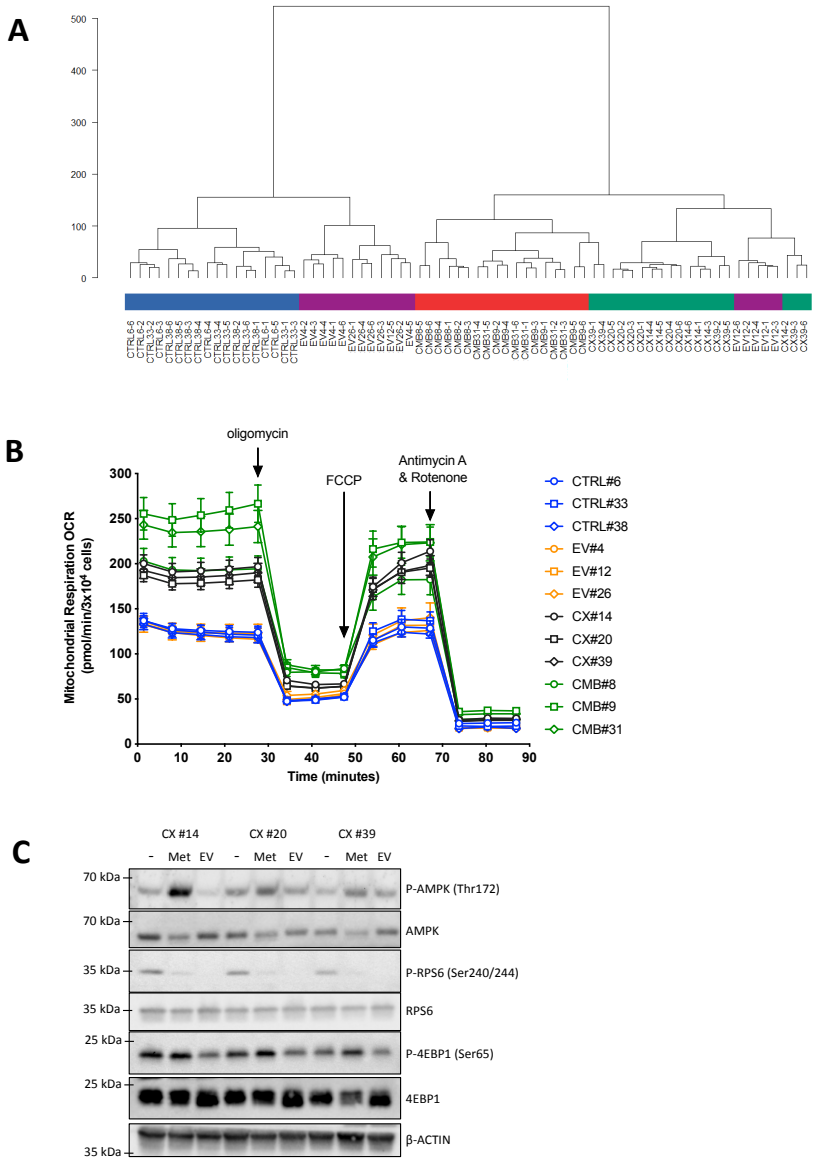

Appendix Figure S2. Characterization of the *in vivo*-derived early-passage Eμ-*Myc* lymphoma cells

(A) Hierarchical clustering analysis of metabolomics data obtained from liquid chromatography (LC)-mass spectrometry (MS) analysis of early-passage cell lines (n=3 with 5-6 technical replicates each). CTRL, EV, CX and CMB: in vivo-derived culture-adapted cells lines as described in Fig 2A. **(B)** Determination of oxygen consumption rate (OCR) using the Seahorse XF96 Extracellular Flux Analyzer in the early-passage Eμ-Myc B-lymphoma cell lines (linked to Fig 2F). A mitochondrial stress test was carried out using sequential addition of oligomycin (1 μM) FCCP (1.5 μM) and rotenone/antimycin (0.5 μM each) injected sequentially. Graphs represent mean± SEM of 6-8 technical replicates of n=3 biological replicates. **(C)** Western blot analysis for indicated proteins in response to 5 mM metformin or 20 nM everolimus treatment for 6 hours (n=3). Actin was used as a loading control.

Appendix Figure S3

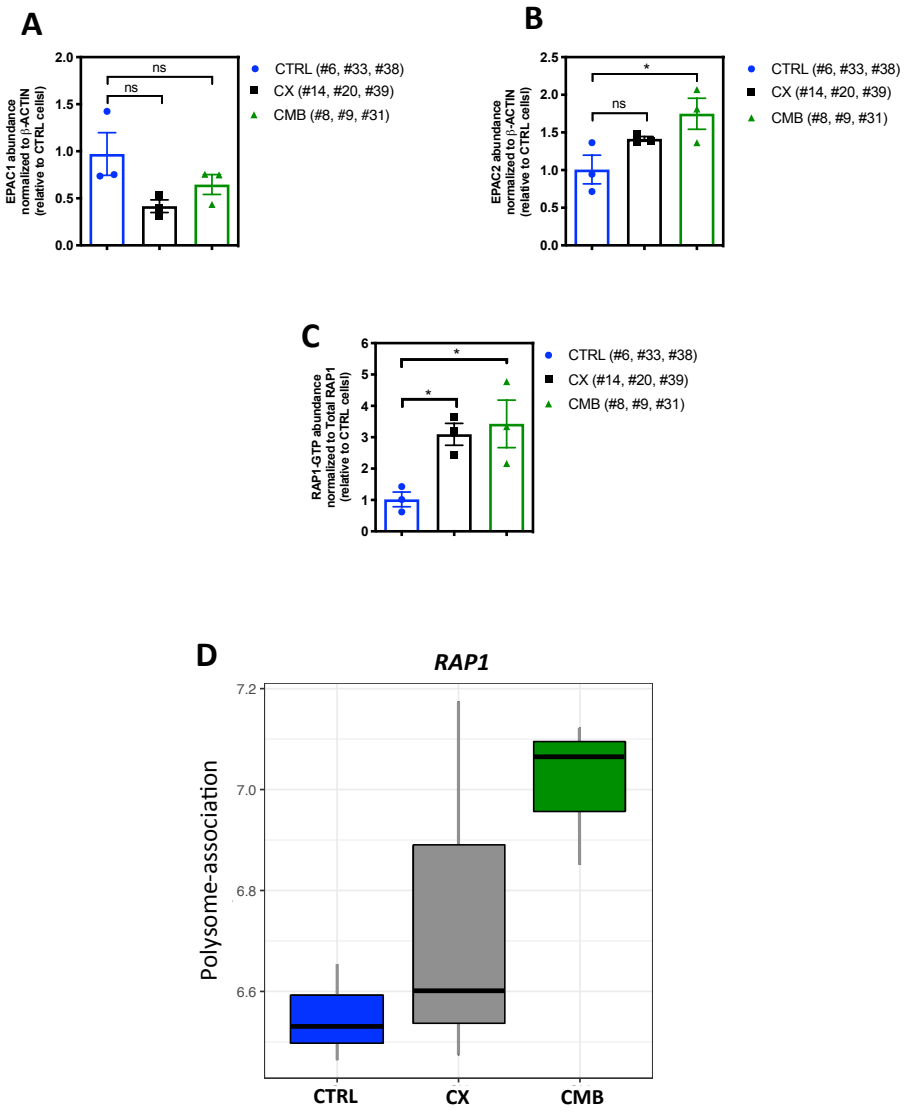

Appendix Figure S3. Analysis of EPAC1/2-RAP1 pathway in drug-naïve versus drug-resistant Eμ-*Myc* lymphoma cells

Quantitation of **(A)** EPAC1, **(B)** EPAC1 and (**C)** RAP1-GTP blots shown in Fig 3C. Graphs represent mean ± SEM of n=3. Data were analysed by one-way ANOVA. ns, not significant, P≥ 0.05; *, P ≤ 0.05. **(D)** Boxplot showing polysomal abundance of mRNA encoding RAP1 protein in early-passage CTRL, CX and CMB Eμ-Myc B-lymphoma cells. CTRL vs. CX; p = 0.0385. CTRL vs. CMB; p = 0.0081 based on limma analysis. The central band corresponds to the median. The lower and upper hinges correspond to the first and third quartiles (the 25th and 75th percentiles). The upper and lower whiskers extend from the hinges to the largest and smallest values no further than 1.5 * inter-quartile range from the hinges, respectively.

APPENDIX TABLES

Appendix Table S1. List of antibodies used in immunoblotting and flow cytometry experiments

Protein	Mass (kDa)	Primary Antibody Details	Primary Antibody Dilution	Secondary Antibody Details
Immunoblotting				
β-ACTIN	42 kDa	MP Biosciences 691002	1:30,000	Goat-α-rabbit HRP[1]
p53	53 kDa	Leica Biosystems	1:1,000	Goat-α-mouse HRP[2]
RPS6	32 kDa	Cell Signalling #2317	1:2,000	Goat-α-mouse HRP[2]
Phospho-RPS6	32 kDa	Cell Signalling #2215	1:2,000	Goat-α-rabbit HRP[1]
Phospho-AMPKα (Thr172)	62 kDa	Cell Signalling #2531	1:1,000	Goat-α-rabbit HRP[1]
AMPKα	62 kDa	Cell Signalling #2532	1:1,000	Goat-α-rabbit HRP[1]
EPAC1	100 kDa	Cell Signalling #4155	1:1,000	Goat-α-mouse HRP[2]
EPAC2	110 kDa	Abcam #193665	1:2,000	Goat-α-rabbit HRP[1]
RAP1	21 kDa	Thermo Fisher Scientific #16120	1:1,000	Goat-α-rabbit HRP[1]
Phospho-PKA substrate (RRXS*/T*)	N.A	Cell Signalling #9624	1:1,000	Goat-α-rabbit HRP[1]
Notes: 1. Goat-α-rabbit horseradish peroxide (HRP) IgG (H+L) (Bio-Rad #170-6515); dilution 1:2,000 2. Goat-α-mouse horseradish peroxide (HRP) IgG (H+L) (Bio-Rad #170-1011); dilution 1:2,000				
Flow cytometry				
B220 (CD45R)-APC	N.A.	Thermo Fisher Scientific 17-0452-82	1:400	N.A.

APPENDIX SUPPLEMENTARY METHODS

5' UTR analysis

For the 5'UTR analysis, 5'UTR sequences were obtained using the biomaRt and org.Mm.eg.db R packages from the Mouse Genome GRCm38.p6. Only 5'UTRs shorter than 500 nucleotides were considered, since others have found that longer 5'UTRs were likely to be false positives. In cases where there were multiple 5'UTR for a single gene, we only considered the shortest 5'UTR. For the resistant study, only genes with FC > 1.5 or < -1.5 were considered, with adjusted $P < 0.05$. One-sided Wilcoxon tests were used to determine significance. Motif enrichment analysis was subsequently performed with the MEME Suite (http://meme-suite.org/).

Bioenergetics analysis using the Seahorse XF96 Extracellular Flux Analyzer

Cells were washed with the assay media (unbuffered DMEM, 5 g/L glucose, 5 mM glutamine, 1 mM sodium pyruvate), before seeding in Seahorse XF96 96-well plates coated with Cell-Tek (3.5 μg/cm^2, Corning) at 2 x 10^5 cells/well in 180 μl of the assay media. The plate was centrifuged at 400g for 5 minutes at room temperature to allow the cells to form a monolayer. The plate was equilibrated in a non-CO2 incubator for 30 minutes prior to assay. The assay protocol consisted of 3 repeated cycles of 3 minutes mixing and 3 minutes of measurement periods, with oxygen consumption rate (OCR) and extracellular acidification rate (ECAR) determined simultaneously. Basal energetics were established after three of these initial cycles, followed by exposure to the ATP synthase inhibitor, oligomycin (1 μM) for three cycles, then p-trifluoromethoxy- phenylhydrazone (FCCP, 1.5 μM), which uncouples oxygen consumption from ATP production, was added for a further three cycles. Finally, the mitochondrial complex III inhibitor antimycin A (0.5 μM) and the complex I inhibitor rotenone (0.5 μM) was added for three cycles. At the completion of each assay, the cells were stained with 10 μM Hoechst. Images were analysed using a Cellomics Cellinsight 1 to determine the cell number per well.

Gas chromatography – mass spectrometry (GC-MS) analysis

Cells were quenched by transferring cell suspensions (5 mL) into 50 mL falcon tubes containing 35 mL ice-cold saline, followed by centrifugation (500 x g, 3 minutes, 0 °C). Once the supernatant was removed, the cells were re- suspended in 1 mL ice-cold saline, transferred to 1.5 mL microfuge tubes, and centrifuged (10,000 x g, 30 seconds, 0 °C). Supernatant was removed completely and metabolites were immediately extracted in 250 μL chloroform:methanol:water ($CHCl_3$:CH_3OH:H_2O, 1:3:1 v/v; monophasic mixture) containing 0.5 nmoles scyllo-inositol as internal standard. The extracts were vortexed (~10 seconds) and incubated on ice for 15 minutes with additional vortexing every 5 minutes. Insoluble material was removed

by centrifugation (10,000 x g, 5 minutes, 0 °C). H_2O was then added to the supernatant to adjust the ratio of $CHCl_3$:CH_3OH:H_2O to 1:3:3 (v/v; biphasic partition). The supernatant was vortexed and centrifuged (10,000 x g, 5 min, 0 °C) to induce phase separation.

The upper (polar) phase was transferred to a fresh microfuge and dried *in vacuo* (30 °C) in 250 µL glass vial inserts. Samples were analyzed by GC-MS as previously described (Masukagami et al, 2017). Briefly, samples were prepared for GC-MS analysis using a Gerstel MPS2 autosampler robot. Polar metabolites were first methoximated with methoxyamine hydrochloride in pyridine (Sigma, 20 µl, 30 mg/ml, 2 hours, 37 °C) and then derivatized with TMS reagent (N,O-bis(trimethylsilyl) trifluoroacetamide containing 1% trimethylchlorosilane (Pierce, 20 µl, 1 hour, 37 °C) and analysed by GC-MS using a VF5 capillary column (Agilent, 30 m, 250 µm inner diameter, 0.25 µm film thickness), with a 10 m inert eziguard. The injector insert and GC-MS transfer line temperatures were 250 and 280 °C, respectively. The oven temperature gradient was programmed as follows: 35 °C (1 minute); then 25 °C /minute to 320 °C; and held at 320 °C for 5 minutes. Metabolites were detected by mass selective detector following electron ionization (-70 eV), where the scan range was 50-600 amu at 9.2 scans/sec. Metabolites were identified and areas integrated based on GC retention time and mass spectra as compared with authentic standards and in conjunction with MSD ChemStation Data Analysis Application (Agilent) using in-house and Wiley metabolite libraries. Statistical analyses were performed using Student *t* test following log transformation and median normalization. Metabolites were considered to be significant if their adjusted p-values after Benjamini-Hochberg correction were less than 0.05.

Liquid chromatography – mass spectrometry (LC-MS)

Cells were quenched by transferring cell suspensions (5 mL) into 50 mL falcon tubes containing 35 mL ice-cold saline, followed by centrifugation (500 x g, 3 minutes, 0 °C). Once the supernatant was removed, the cells were re- suspended in 1 mL ice-cold saline, transferred to 1.5 mL microfuge tubes, and centrifuged (10,000 x g, 30 seconds, 0 °C). Supernatant was removed completely and metabolites were immediately extracted using ice-cold 80% acetonitrile:water (v/v) containing internal standards (^{13}C-Sorbitol and ^{13}C- Valine; final concentration 4 µM both). Metabolites in the cell extracts were analyzed by high-performance liquid chromatography mass spectrometer (LC-MS) as previously described (Masukagami et al, 2017). Briefly, metabolites were separated on an Agilent Technologies 1200 series HPLC system (Agilent Technologies, Santa Clara, US, USA) using a SeQuant ZIC–pHILIC (5 µm polymer) PEEK 150 x 4.6 mm metal-free HPLC column maintained at 25°C with solvent A (20 mM $(NH_4)_2CO_3$, pH 9.0; Sigma- Aldrich) and solvent B (100% acetonitrile) at a flow rate of 300 µl/minute. Metabolites were detected by mass spectrometry on an Agilent Technologies 6545A series quadrupole time of flight mass spectrometer (QTOF MS) using an electrospray ionization source (ESI). LC-MS data

was collected in negative MS mode. Data processing was performed using Agilent MassHunter workstation quantitative analysis for TOF software (Version B.07.00/Build 7.0.457.0). Metabolite identification was based on accurate mass, retention time and authentic chemical standards at level 1 confidence according to the Fiehn's Metabolomics Standard Initiative.

REFERENCES

Masukagami Y, De Souza D, Dayalan S, Bowen C, O'Callaghan S, Kouremenos K, Nijagal B, Tull D, Tivendale K, Markham P (2017) Comparative metabolomics of Mycoplasma bovis and Mycoplasma gallisepticum reveals fundamental differences in active metabolic pathways and suggests novel gene annotations. *MSystems* **2:** e00055-00017